Revisiting the Thickness of the Air-Water Interface from Two Extremes of Interface Hydrogen Bond Dynamics

Gang Huang*[1, a)] and Jie Huang*[2, b)]
[1)] *Institute of Theoretical Physics, Chinese Academy of Sciences, Zhongguancun East Road 55, 100190 Beijing, China*
[2)] *Department of Applied Physics, Aalto University, Helsinki FI-00076, Finland*

(Dated: 2 April 2024)

The air-water interface plays a crucial role in many aspects of science, because of its unique properties, such as a two-dimensional hydrogen bond (HB) network and completely different HB dynamics compared to bulk water. However, accurately determining the boundary of interfacial and bulk water, that is, the thickness of the air-water interface, still challenges experimentalists. Various simulation-based methods have been developed to estimate the thickness, converging on a range of approximately 3 to 10 Å. In this study, we introduce a novel approach, grounded in density functional theory-based molecular dynamics (DFTMD) simulations, to measure the air-water interface thickness, offering a different perspective based on prior research. To capture realistic HB dynamics in the air-water interface, two extreme scenarios of the interface HB dynamics are obtained: one underestimates the interface HB dynamics, while the other overestimates it. Surprisingly, our results suggest that the interface HB dynamics in both scenarios converge as the thickness of the air-water interface increases to 4.0 Å. This convergence point, indicative of the realistic interface thickness, is confirmed by our calculation of anisotropic decay of OH stretch at the air-water interface and supported by the results from recent *ab initio* molecular dynamics simulations.

I. INTRODUCTION

The air-water interface has been the subject of extensive study due to its ubiquity in nature and its unusual macroscopic properties as a model system for aqueous hydrophobic interfaces[1–16]. It is widely accepted that water molecules behave in a completely different manner at the interface than in the bulk phase[17–19].

Advances in the study of hydrogen bond (HB) dynamics at the air-water interface have been significant. Liu et al.[20] used molecular dynamics (MD) simulations to demonstrate faster HB breaking and forming at the interface than bulk water, attributed to quicker translational diffusion. From sum frequency generation (SFG) vibrational spectroscopy, Gan et al.[21] found that at the air-water interface, singly hydrogen (H)-bonded water molecules align almost parallel to the interface with limited orientational variation, while doubly H-bonded donor molecules orient their dipole vectors away from the liquid phase, highlighting diverse behaviors among interfacial water molecules. Almost concurrently, through time-resolved SFG vibrational spectroscopy, McGuire and Shen[22] observed ultrafast vibrational dynamics at the interface, noting that the relaxation behaviors of interfacially bonded OH stretch modes on sub-picosecond timescales were akin to those in bulk water, encompassing spectral diffusion, vibrational relaxation, and thermalization. Pioneering work by Tahara's group[23,24], which presented the first two-dimensional heterodyne-detected vibrational SFG (2D HD-VSFG) spectra of the OH stretch region at the interface, highlighted diverse behaviors among interfacial HB OH groups. Subsequent studies, including those by Jeon et al.[25] and Ojha and Kühne[26], have used MD and *ab initio* MD (AIMD) simulations to explore the structure and dynamics of interfacial water, uncovering weaker H-bonds and faster vibrational spectral dynamics of free OH groups compared to H-bonded OH groups at the interface. These collective insights enhance our understanding of the vibrational energy relaxation, HB dynamics, and interactions of water molecules at the air-water interface. Building upon this knowledge of interfacial behavior, significant efforts have also been directed towards quantifying the physical characteristics of the interface, including its thickness, which plays a crucial role in understanding its molecular interactions and behavior.

The air-water interface thickness has been measured via ellipsometry[27–29], relative permittivity measurements[30], X-ray reflectivity[31,32], SFG spectroscopy[23,33–41], classical MD simulations[20,42–51] and the AIMD simulations[25,41,52–55] to mention just a few. There is a consensus that the thickness of the air-water interface is about 3 to 10 Å[42,43,45–47,52,54,56–59]. Nonetheless, accurately determining the thickness remains experimentally challenging. The MD and Monte Carlo (MC) simulations of the air-water interface yield molecular-level information not readily available in experiments. These simulations, which utilize various intermolecular potential functions, have played a crucial role in estimating the thickness[41,60–67]. Additionally, density functional theory-based MD (DFTMD) simulations[52,68–73] also offer a predictive platform for understanding density profiles and determining the thickness of the air-liquid interfaces[52,54,74,75].

Inspired by the above experimental and simulation results, and with the motivation of capturing realistic HB dynamics at interfaces, we have designed an approach based on two extreme scenarios of interface HB dynamics. In the first scenario, for the set of molecules located in the interface layer at a given sampling time, we use the Luzar-Chandler (LC) HB population operator[76] to obtain the HB dynamics of these interface molecules. In the second scenario, taking inspiration

[a)] Electronic mail: huanggang@itp.ac.cn
[b)] Electronic mail: jie.huang@aalto.fi

from Luzar and Chandler's HB population and the characteristic function introduced by Giberti and Hassanali[77], we have developed an interface HB (IHB) population operator. This operator aims to provide a refined understanding of HB dynamics specifically at the interface.

The Luzar-Chandler HB population is utilized to describe whether a pair of labeled molecules form H-bonds. And the characteristic function developed by Giberti and Hassanali describes whether a specific molecule belongs to the interface region. Therefore, our newly defined interface HB population can describe whether a labeled pair of molecules is within the interface *and* connected by H-bonds at any given moment. This dual condition provides a more detailed understanding of interfacial HB dynamics.

Due to the thermal motion of water molecules, two scenarios may occur. In the first scenario, the water molecules under observation might transition into the bulk phase. In the second scenario, if a water molecule resides in the interface region *and* its H-bonded partner moves outside the interface area, then such a pair of molecules will no longer be of concern. Based on the study of interfacial water dynamics by Liu et al.[20], Gan et al.[21], Singh et al.[23] and Jeon et al.[25], as well as the investigation into the time-dependent spectral evolution of H-bonded and free water molecules by Ojha and Kühne[26], our approach indicates that the HB dynamics derived from the first scenario will be slower the genuine interfacial HB dynamics. Conversely, the one obtained from the second scenario will exhibit a faster dynamics than the genuine one.

Building upon the foundation laid by methods reliant on the density criterion[1,63–66,78–82], our approach introduces an alternative way of determining interface thickness through the analysis of the convergence of interfacial HB dynamics properties. This approach effectively bypasses the necessity of accounting for liquid density. As such, it offers another perspective for measuring the thickness of air-water interfaces. Furthermore, the principles underlying our approach hold potential for application to a broader range of systems, such as solution interfaces and ion shells, offering a flexible tool for interface studies.

II. METHODS

Due to molecular motions, the identity of molecules at the interface changes with time, and generally useful procedures for identifying interfaces must accommodate these motions. The air-water boundary is modeled with the Willard-Chandler instantaneous surface[48,75,83]. Figure 1 illustrates the obtained interfaces for one configuration of a slab of water.

For the slab in the cuboid simulation box, an imaginary surface $\mathbf{S}'(t)$ is obtained by translating the surface $\mathbf{S}(t)$ along the system's normal (into bulk) to a distance d. The region between the two surfaces $\mathbf{S}(t)$ and $\mathbf{S}'(t)$ is defined as *the air-water interface*. Below we will combine two extreme scenarios to investigate the HB dynamics at the instantaneous air-water interface.

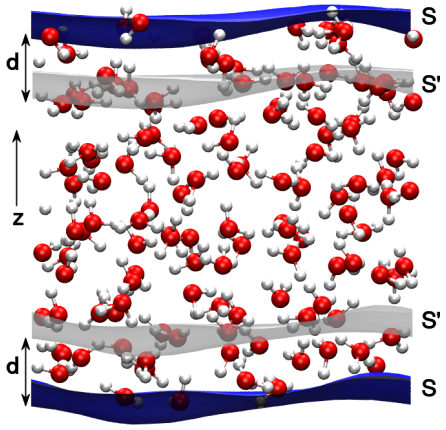

FIG. 1. A slab of water with the instantaneous surface **S** represented as a blue mesh on the upper and lower phase boundary. The grey surface, which represents an imaginary interface $\mathbf{S}'$, is obtained by translating the surface to the inside of the system along the normal (z-axis) by distance d. This distance d is then utilized to measure the thickness of the air-water interface.

A. Scenario 1: HB dynamics based on the Luzar-Chandler HB population $h[\mathbf{r}(t)]$

As the first scenario we use the Luzar-Chandler HB population operator[76] and employ a technique that samples water molecules right at the instantaneous interface for certain sampling time points. During the t_{traj} period, most water molecules only undergo thermal motion near their equilibrium position. However, a small number of molecules that are at the interface at time t may enter the bulk phase at a later time. Due to the inclusion of H-bonds in the bulk phase, this scenario tends to *underestimate* the breaking rate of the H-bonds at the interface. This Luzar-Chander HB population-based method includes three steps as follows.

1. Sub-trajectories: Sub-trajectories with a specific length of time, $t_{\text{traj}} \sim 10$ ps are selected. Here, t_{traj} is long enough to observe HB dynamics but short enough that the molecules do not complete their transition across the interface[84].

2. Sampling: At multiple, evenly spaced moments within t_{traj}, we identify a layer at the interface of a specified thickness d (see Fig. 1) and select the water molecules within this layer for analysis. For each of these moments, the Luzar-Chandler HB population-based correlation functions[76] for these molecules across the sub-trajectory t_{traj} are calculated.

3. Statistics: The average properties over all sampled moments and all sub-trajectories are calculated.

For details on this LC HB operator-based method (LC method), see Appendix C.

B. Scenario 2: HB dynamics based on interface HB population $h^{(\mathbf{s})}[\mathbf{r}(t)]$

To capture the other extreme of interfacial HB dynamics, after determining the instantaneous interface, we introduce an interface HB population operator $h^{(\mathrm{s})}[\mathbf{r}(t)]$ as follows: It has a

value of 1 when a tagged molecular pair i, j are H-bonded *and* both molecules are at the interface with a thickness d, and 0 otherwise:

$$h^{(s)}[\mathbf{r}(t)] = \begin{cases} 1 & \mathbf{r}_i \in \mathscr{I}(d;t), \mathbf{r}_j \in \mathscr{I}(d;t), \\ & j \in \mathscr{S}_i(t); \\ 0 & \text{otherwise}, \end{cases} \quad (1)$$

where $\mathscr{S}_i(t)$ denotes the set of water molecules that are H-bonded with molecule i at time t, and $\mathscr{I}(d;t)$ is the instantaneous interface layer with thickness d at time t, as defined previously. The definition of $h^{(s)}$ combines the Luzar-Chandler's HB population[76,85] h and the characteristic function introduced by Giberti and Hassanali[77]. Then the correlation function $c^{(s)}(t)$ that describes the fluctuation of H-bonds *at the interface*:

$$c^{(s)}(t) = \langle h^{(s)}(0)h^{(s)}(t)\rangle / \langle h^{(s)}\rangle, \quad (2)$$

can be obtained.

Similar to functions $n(t)$ and $k(t)$ in Ref. 76 (Eq.s A1 and A2 in Appendix A), the corresponding correlation function

$$n^{(s)}(t) = \langle h^{(s)}(0)[1-h^{(s)}(t)]h^{(d,s)}\rangle / \langle h^{(s)}\rangle, \quad (3)$$

and interface reactive flux function

$$k^{(s)}(t) = -dc^{(s)}(t)/dt \quad (4)$$

are obtained. The $h^{(d,s)}(t)$ is 1 when a tagged pair of water molecules i, j is *at the interface* and the inter-oxygen distance between the two molecules is less than the cutoff radius r_{OO}^{c} at time t, and 0 otherwise, i.e.,

$$h^{(d,s)}[\mathbf{r}(t)] = \begin{cases} 1 & \mathbf{r}_i \in \mathscr{I}(d;t), \mathbf{r}_j \in \mathscr{I}(d;t), \\ & |\mathbf{r}_i - \mathbf{r}_j| < r_{OO}^{c}; \\ 0 & \text{otherwise}. \end{cases} \quad (5)$$

Therefore, $n^{(s)}(t)$ represents the probability at time t that a tagged pair of initially H-bonded water molecules at the interface are unbonded but remain at the interface and separated by less than r_{OO}^{c}; $k^{(s)}(t)$ measures the effective decay rate of H-bonds at the interface. The functions defined in Eq.s 2–4 are used to determine the reaction rate constants of breaking and reforming and the lifetimes of H-bonds at the interface by[73,76]

$$k^{(s)}(t) = kc^{(s)}(t) - k'n^{(s)}(t).$$

In this IHB scenario, choosing the water molecules and H-bonds at the interface is accurate. However, for some special H-bonds, if it connects such two water molecules, one is at the interface and the other is in bulk water, the HB breaking reaction rate of such H-bonds will be increased. Therefore, in contrast to the LC method used in scenario 1, the IHB method used in this scenario *overestimates* the HB breaking rate constant.

The actual HB dynamics at the interface are expected to lie between the results obtained by the LC method and the IHB method. Consequently, by integrating these two scenarios, we can achieve a more precise characterization of HB dynamics at the interface.

III. RESULTS AND DISCUSSIONS

In this section, we implement our two-extreme approach to two distinct system properties: HB population auto-correlation functions and HB reaction rate constants. We then determine the thickness of the air-water interface based on each of these properties.

A. HB population auto-correlation functions

Figure 2 illustrates the dynamic evolution of $c(t)$ and $c^{(s)}(t)$ for various values of d. When d is equal to or greater than 4.0 (Å), the time evolution curves of $c(t)$ and $c^{(s)}(t)$ become largely invariant to further increases in d. This shows that one can calculate the thickness of the interface under different conditions with the help of the dependence of the correlation function on d. Analyzing both scenarios, it is evident that the decay rate of the correlation function $c^{(s)}(t)$ in scenario 2 (IHB) surpasses that in scenario 1 (LC).

Figure 3 shows the d-dependence of the correlation functions at three reference time points $t^* = 1, 2, 5$ (ps). It shows the d-dependence clearly from another angle: we selected the three reference time intervals on the t-axis in Fig. 2 and recorded the values of the correlation functions, $c(t)$ and $c^{(s)}(t)$, at these time intervals for each d. Comparing $c(t)$ and $c^{(s)}(t)$ in Fig. 3, $c(t)$ is always slightly larger than $c^{(s)}(t)$ for the same d.

In Fig. 3, both $c(t^*)$ and $c^{(s)}(t^*)$ increase as d increases, and eventually their change rates approach 0 when d is large enough. Since $c(t)$ and $c^{(s)}(t)$ are the upper and lower bounds of the real interface correlation functions $c^r(t^*)$ respectively. It logically follows that the d-dependence of $c^r(t^*)$ has the same changing trend. Then we have the equations $\mathrm{d}C/\mathrm{d}d = 0$, for $c(t^*)$ and $c^{(s)}(t^*)$, with respect to d. For $C = c(t^*)$ and $C = c^{(s)}(t^*)$, we can find solutions d_{f1} and d_{f2}, respectively. Here d_{f1} and d_{f2} are the thickness of the air-water interface obtained from the LC method and the IHB method, respectively. Then $d_f = (d_{f1} + d_{f2})/2$ is obtained as the thickness of the interface for a given t^*.

The correlations $c(t^*)$ and $c^{(s)}(t^*)$ respectively describe the relaxation characteristics of HB dynamics within the interface. For both the LC and IHB methods, the values of $c(t^*)$ and $c^{(s)}(t^*)$ no longer change significantly with the increase of d, when d increases to 4.0 (Å), ie., $d_{f1} \approx d_{f2} = 4.0$ (Å). Therefore, we obtain the thickness of the air-water interface in the simulations, i.e., $d_f = 4.0$ (Å). Note that the ADH criterion of H-bonds is used here. Such an observation is in harmony with the findings based on the AHD criterion, as elaborated in Appendix A.

B. HB reaction rate constants

We further examined how the reaction rate constants of H-bonds at the air-water interface vary with d. For further details

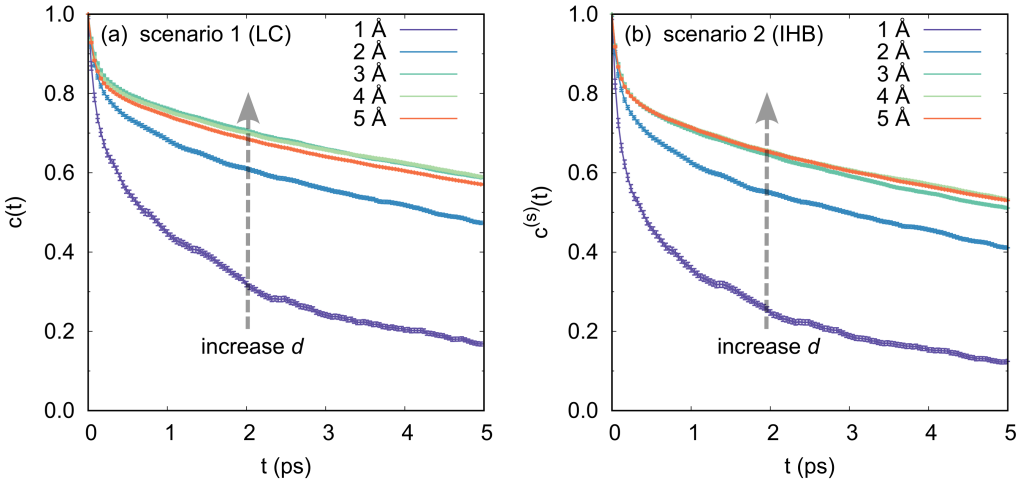

FIG. 2. The $c(t)$ and $c^{(s)}(t)$ for interface H-bonds with different thickness d obtained from the ADH criterion of HB definition for (a) scenario 1 (LC); (b) scenario 2 (IHB). Two features can be found: (i). As d increases, both $c(t)$ and $c^{(s)}(t)$ eventually approach a stable function. (ii). The decay rate of $c^{(s)}(t)$ in scenario 2 surpasses $c(t)$ in scenario 1. This is visually represented by two dashed directed line segments, positioned identically to the graphs.

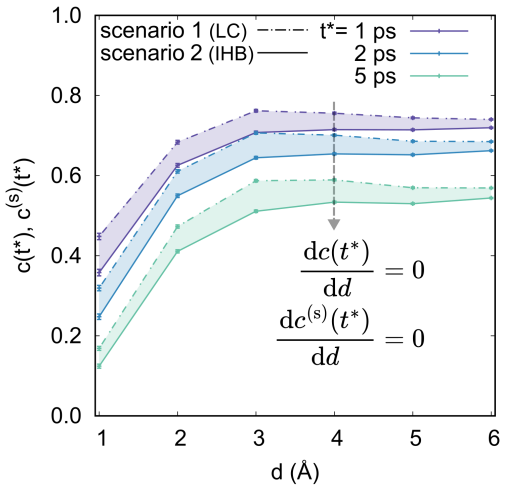

FIG. 3. The d-dependence of the correlation functions at three reference time points $t^* = 1, 2, 5$ (ps), revealing key insights into the dynamics of the air-water interface: (i). As d increases, both $c(t^*)$ and $c^{(s)}(t^*)$ show an upward trend, with their rates of change gradually approaching 0. (ii). For each t^*, $c(t)$ is always slightly larger than $c^{(s)}(t)$ for the same d. (iii). The thickness $d_f = 4.0$ (Å) of the air-water interface is obtained from the d-dependence of $c(t^*)$ and $c^{(s)}(t^*)$, obtained by the LC method (dot-dashed lines) and the IHB method (solid lines), respectively.

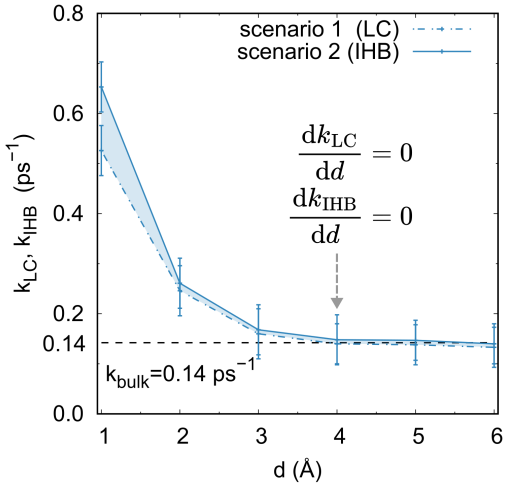

FIG. 4. The breaking HB reaction rate constants k_{LC} and k_{IHB} obtained by the IHB and LC methods respectively. (i). Both constants, k_{LC} and k_{IHB}, decrease monotonically to the HB breaking rate k_{bulk} for the bulk water as d increases. (ii). k_{LC} is always smaller than k_{IHB} for the same d. (iii). The thickness $d_f' = 4.0$ (Å) of the air-water interface is obtained from the d-dependence of the rate constant k_{IHB} and k_{LC}, obtained by the IHB method and the LC method, respectively.

regarding the HB reaction rate constants, please refer to Appendix B.

In Fig. 4, we compare the breaking HB reaction rate constants[76,86], k_{LC} and k_{IHB}, obtained by the IHB and LC methods, respectively. We found that both constants, k_{LC} and k_{IHB}, decrease monotonically as d increases. When d is large, both rate constants k_{IHB} and k_{LC} also no longer change with d. In addition, the HB breaking rate k_{bulk} for the *bulk* water is also drawn as a reference. As d increases, both k_{LC} and k_{IHB} gradually close to the rates k_{bulk}. It also shows that the HB beaking rate constant k_{IHB} is relatively larger than k_{LC}. This difference is related to the definitions of HB populations, $h(t)$ and $h^{(s)}(t)$. The definition of $h^{(s)}(t)$ makes the HB break rate at the interface increase. The LC method, which is based on Luzar-Chandler HB population $h(t)$, retains the original rate constant of H-bonds, but it may include the contribution of bulk water molecules to the rate constant.

Similar to the HB auto-correlation functions, we have the equations $\mathrm{d}K/\mathrm{d}d = 0$, for k_{IHB} and k_{LC}, with respect to d. For

$K = k_{\mathrm{IHB}}$ and $K = k_{\mathrm{LC}}$, we can find solutions d'_{f1} and d'_{f2}, respectively. Here d'_{f1} and d'_{f2} are also the HB reaction rate-based thickness of the interface obtained from the LC and IHB method, respectively. Then we obtain the thickness of the real air-water interface as $d'_f = (d'_{f1}, d'_{f2})/2 \approx 4.0$ (Å). This result is supported by our calculation of the d-dependence of the HB reforming rate constants, ie., k'_{LC} and k'_{IHB}. For more details, please refer to Fig. B7 in Appendix B).

C. Orientational relaxation of the OH stretch and other supports

To verify our conclusion on the thickness of the air-water interface from the interfacial HB dynamics, we calculated the orientational relaxation of the OH stretch from the perspective of anisotropy decay. As shown in Fig. 5, the values of the orientational correlation function $C_2(t)$ at four reference times $t^* = 1, 2, 5$ (ps) are plotted. It can be seen that when the interface thickness d is small, the OH orientational relaxation time τ_2 of the $C_2(t)$ increases linearly with d. The τ_2 for the neat water surface is 1.4 to 2.0 (ps), with std. error $\delta d = 0.1$ (ps), which is consistent with the vibrational relaxation time of the free OH for the neat water[87].

Similar to the HB population correlation functions $c(t)$ and $c^{(\mathrm{s})}(t)$ and the HB reaction rates, k_{LC} and k'_{LC}, and k_{IHB} and k'_{IHB}, as d increases, $C_2(t^*)$ and τ_2 converges to a fixed value, which characterizes the decay time of the orientation relaxation process of OH bonds in bulk water. From the convergence trend of τ_2 in Fig. 5(b), we find that at the interface with a thickness greater than 4.0 Å, the OH orientation relaxation of the air-water interface is no longer different from bulk water. Therefore, we arrive at a consistent conclusion on the issue of estimating the thickness of the air-water interface, from the perspective of HB dynamics and OH reorientation relaxation. Furthermore, the interface thickness aligns with values obtained through experimental measurements and AIMD simulations, as detailed in Table I.

IV. CONCLUSIONS

In this study, we have developed a "two-extremes" approach to investigate the HB dynamics at the air-water interface and to determine the interface's thickness. One extreme scenario underestimates the HB breaking rate constant, while the other overestimates it, implying that each scenario provides only a partial insight into the interfacial HB dynamics. Subsequently, based on the DFTMD simulations, we have applied our approach to two distinct system properties: HB relaxation and HB reaction rate constants at the air-water interface. Our results across all these properties indicate that the predictions from both extreme scenarios converge as the thickness of the air-water interface increases to 4.0 Å. Thus, we have reason to believe the thickness, which falls between these two extremes, converges at this critical value.

This work introduces an approach to complement existing ones for investigating the air-water interface from a fresh perspective. Through HB dynamics of the air-water interface, interfacial properties, such as thickness in this case, can be obtained through a method analogous to the squeeze theorem. Beyond the scope of HB dynamics, this approach can be extended to other properties like molecular orientation distribution[88,89] and SFG spectrum[11,13,41], as well as other solution interfacial surfaces where statistical properties of the interface and bulk phase differ significantly. Looking ahead, our study could also inspire researchers to examine the hydration shells of ions, and then study the effects of ions through HB dynamics.

ACKNOWLEDGMENTS

This work was supported by the CSC | Chinese Government Scholarship (No. 2011113214). We thank Marialore Sulpizi for the useful discussion. The simulations were performed on the Mogon ZDV cluster in Mainz and on the Cray XE6 (Hermit) at the HRLS supercomputing center in Stuttgart.

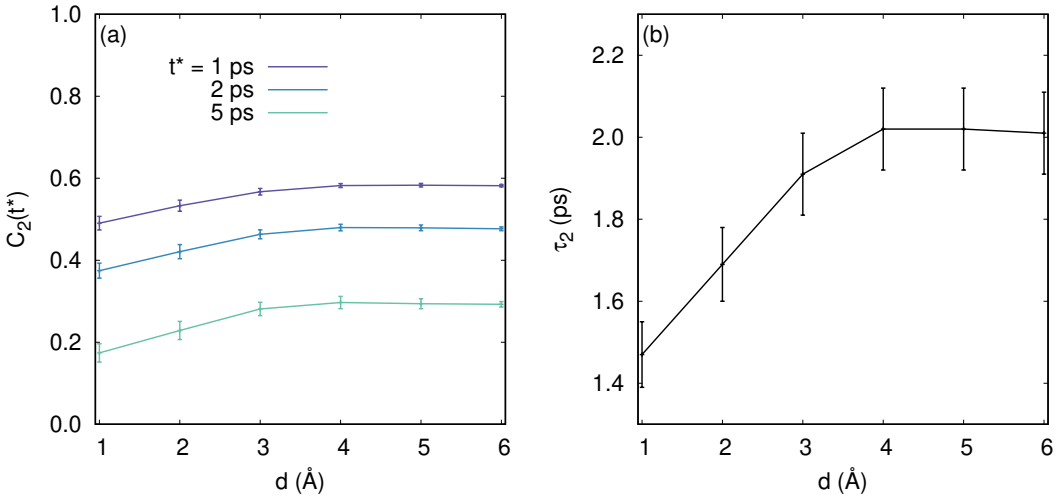

FIG. 5. The d-dependence of (a) $C_2(t^*)$ and (b) $\tau_2(t^*)$ for water molecules at the air-water interface with $t^* = 1, 2, 5$ (ps), respectively. As d increases to $d = 4$ (Å), $C_2(t^*)$ and τ_2 converge to a fixed value, respectively.

TABLE I. The air-water interface thickness obtained by experiments and computer simulations ("-" denotes without using "10–90" thickness).

Method	Thickness Notation	T (K)	d (Å)
Ellipsometry (Rayleigh)	-	293.15	3.0
Ellipsometry (Raman and Ramdas [27])	-	293	5.0
Ellipsometry (McBain, Bacon, and Bruce [28])	-	293	$\geq$2.26
Ellipsometry (Kinosita and Yokota [29])	-	293	7.1
X-Ray Reflectivity(Braslau *et al.* [32])	-	298	3.24$\pm$ 0.05
MD (TIP4P/FQ, Liu *et al.*[20])	10–90	298.15	3.5
MD (TIP4P-POL2, Kuo *et al.*[42])	10–90	298	3.9
MD (SPC-FW, Wick *et al.*[43])	10–90	298	3.2
MD (D-C, Wick *et al.*[43])	10–90	298	3.2
MD (TIP4P, Wick *et al.*[43])	10–90	298	3.4
MD (SPC/E, Fan *et al.*[46])	10–90	300	6.0
MD (SPC/E, Willard and Chandler[48])	10–90	298	8.0
MD (SPC/E, Vila Verde *et al.*[49])	10–90	300	3.27
MD (TIP4P/2005, Vila Verde *et al.*[49])	10–90	300	3.05
CPMD/BLYP (Kuo *et al.*[42])	10–90	300	1.7
BOMD/BLYP-D (Kühne et al.[52])	10–90	300	3.8
BOMD/BLYP-D2 (Pezzotti *et al.*[75])	10–90	315	3.5
BOMD/BLYP-D3 (Jeon *el al.*[25])	10–90	298	$\sim$3.0
BOMD/BLYP-D3/LC&IHB (this work)	-	300	4.0

[1] A. Morita and J. T. Hynes, "A theoretical analysis of the sum frequency generation spectrum of the water surface," Chem. Phys. **258**, 371–390 (2000).

[2] P. Jungwirth and D. J. Tobias, "Molecular Structure of Salt Solutions: A New View of the Interface with Implications for Heterogeneous Atmospheric Chemistry," J. Phys. Chem. B **105**, 10468–10472 (2001).

[3] K. R. Wilson, R. D. Schaller, D. T. Co, R. J. Saykally, B. S. Rude, T. Catalano, and J. D. Bozek, "Surface relaxation in liquid water and methanol studied by x-ray absorption spectroscopy," J. Chem. Phys. **117**, 7738–7744 (2002).

[4] E. A. Raymond, T. L. Tarbuck, M. G. Brown, and G. L. Richmond, "Hydrogen-Bonding Interactions at the Vapor/Water Interface Investigated by Vibrational Sum-Frequency Spectroscopy of HOD/H_2O/D_2O Mixtures and Molecular Dynamics Simulations," J. Phys. Chem. B **107**, 546–556 (2003).

[5] Y. R. Shen and V. Ostroverkhov, "Sum-Frequency Vibrational Spectroscopy on Water Interfaces: Polar Orientation of Water Molecules at Interfaces," Chem. Rev. **106**, 1140–1154 (2006).

[6] M. Smits, A. Ghosh, M. Sterrer, M. Müller, and M. Bonn, "Ultrafast vibrational energy transfer between surface and bulk water at the air-water interface," Phys. Rev. Lett. **98**, 098302 (2007).

[7] M. Sovago, R. K. Campen, G. W. H. Wurpel, M. Müller, H. J. Bakker, and M. Bonn, "Vibrational response of hydrogen-bonded interfacial water is dominated by intramolecular coupling," Phys. Rev. Lett. **100**, 173901 (2008).

[8] M. Sovago, R. Kramer Campen, H. J. Bakker, and M. Bonn, "Hydrogen bonding strength of interfacial water determined with surface sum-frequency generation," Chem. Phys. Lett. **470**, 7–12 (2009).

[9] I. V. Stiopkin, C. Weeraman, P. A. Pieniazek, F. Y. Shalhout, J. L. Skinner, and A. V. Benderskii, "Hydrogen Bonding at the Water Surface Revealed by Isotopic Dilution Spectroscopy," Nature **474**, 192 (2011).

[10] C.-S. Hsieh, R. K. Campen, A. C. Vila Verde, P. Bolhuis, H.-K. Nienhuys, and M. Bonn, "Ultrafast reorientation of dangling oh groups at the air-water interface using femtosecond vibrational spectroscopy," Phys. Rev. Lett. **107**, 116102 (2011).

[11] S. Nihonyanagi, T. Ishiyama, T.-K. Lee, S. Yamaguchi, M. Bonn, A. Morita, and T. Tahara, "Unified Molecular View of the Air/Water Interface Based on Experimental and Theoretical $\chi^{(2)}$ Spectra of an Isotopically Diluted Water Surface," J. Am. Chem. Soc. **133**, 16875–16880 (2011).

[12] P. C. Singh, S. Nihonyanagi, S. Yamaguchi, and T. Tahara, "Interfacial water in the vicinity of a positively charged interface studied by steady-state and time-resolved heterodyne-detected vibrational sum frequency generation," J. Chem. Phys. **141**, 18C527 (2014).

[13] S. Nihonyanagi, R. Kusaka, K.-i. Inoue, A. Adhikari, S. Yamaguchi, and T. Tahara, "Accurate determination of complex $\chi^{(2)}$ spectrum of the air-water interface," J. Chem. Phys. **143**, 124707 (2015).

[14] T. Ishiyama, "Energy relaxation path of excited free OH vibration at an air/water interface revealed by nonequilibrium ab initio molecular dynamics simulation," J. Chem. Phys. **154**, 104708 (2021).

[15] M. Ahmed, S. Nihonyanagi, and T. Tahara, "Ultrafast vibrational dynamics of the free OD at the air/water interface: Negligible isotopic dilution effect but large isotope substitution effect," J. Chem. Phys. **156**, 224701 (2022).

[16] A. Omranpour, D. Hijes, P. Montero, J. Behler, and C. Dellago, "Perspective: Atomistic simulations of water and aqueous systems with machine learning potentials," arXiv preprint arXiv:2401.17875 (2024).

[17] C. Lee, J. A. McCammon, and P. J. Rossky, "The structure of liquid water at an extended hydrophobic surface," J. Chem. Phys. **80**, 4448–4455 (1984).

[18] L. X. Dang and T.-M. Chang, "Molecular dynamics study of water clusters, liquid, and liquid-vapour interface of water with many-body potentials," J. Chem. Phys. **106**, 8149 (1997).

[19] C.-S. Hsieh, R. K. Campen, M. Okuno, E. H. G. Backus, Y. Nagata, and M. Bonn, "Mechanism of vibrational energy dissipation of free oh groups at the air-water interface," Proceedings of the National Academy of Sciences **110**, 18780–18785 (2013).

[20] P. Liu, E. Harder, and B. J. Berne, "Hydrogen-Bond Dynamics in the Air-Water Interface," J. Phys. Chem. B **109**, 2949–2955 (2005).

[21] W. Gan, D. Wu, Z. Zhang, R.-r. Feng, and H.-f. Wang, "Polarization and experimental configuration analyses of sum frequency generation vibrational spectra, structure, and orientational motion of the air/water interface," J. Chem. Phys. **124**, 114705 (2006).

[22] J. A. Mcguire and Y. R. Shen, "Ultrafast vibrational dynamics at water interfaces," Science **313**, 1945–1948 (2006).

[23] P. C. Singh, S. Nihonyanagi, S. Yamaguchi, and T. Tahara, "Communication: Ultrafast vibrational dynamics of hydrogen bond network terminated at the air/water interface: A two-dimensional heterodyne-detected vibrational sum frequency generation study," J. Chem. Phys. **139**, 161101 (2013).

[24] K.-i. Inoue, T. Ishiyama, S. Nihonyanagi, S. Yamaguchi, A. Morita, and T. Tahara, "Efficient spectral diffusion at the air/water interface revealed by femtosecond time-resolved heterodyne-detected vibrational sum frequency generation spectroscopy," J. Phys. Chem. Lett. **7**, 1811–1815 (2016).

[25] J. Jeon, C.-S. Hsieh, Y. Nagata, M. Bonn, and M. Cho, "Hydrogen bonding and vibrational energy relaxation of interfacial water: A full DFT molecular dynamics simulation," J. Chem. Phys. **147**, 044707 (2017).

[26] D. Ojha and T. Kühne, "Hydrogen bond dynamics of interfacial water molecules revealed from two-dimensional vibrational sum-frequency generation spectroscopy," Sci. Rep. **11**, 2456 (2021).

[27] C. Raman and L. Ramdas, "On the thickness of the optical transition layer in liquid surfaces," Phil. Mag. **3**, 220 (1927).

[28] J. W. McBain, R. C. Bacon, and H. D. Bruce, "Optical surface thickness of pure water," J. Chem. Phys. **7**, 818–823 (1939).

[29] K. Kinosita and H. Yokota, "Temperature dependence of the optical surface thickness of water," J. Phys. Soc. Japan **20**, 1086 (1965).

[30] L. Fumagalli, A. Esfandiar, R. Fabregas, S. Hu, P. Ares, A. Janardanan, Q. Yang, R. B., T. Taniguchi, K. Watanabe, G. Gomila, K. S. Novoselov, and A. K. Geim, "Anomalously low dielectric constant of confined water," Science **360**, 1339–1342 (2018).

[31] A. Braslau, M. Deutsch, P. S. Pershan, A. H. Weiss, J. Als-Nielsen, and J. Bohr, "Surface roughness of water measured by x-ray reflectivity," Phys. Rev. Lett. **54**, 114–117 (1985).

[32] A. Braslau, P. S. Pershan, G. Swislow, B. M. Ocko, and J. Als-Nielsen, "Capillary waves on the surface of simple liquids measured by x-ray reflectivity," Phys. Rev. A **38**, 2457–2470 (1988).

[33] R. Superfine, J. H. Huang, and Y. R. Shen, "Nonlinear Optical Studies of the Pure Liquid/Vapor Interface: Vibrational Spectra and Polar Ordering," Phys. Rev. Lett. **66**, 1066–1069 (1991).

[34] Q. Du, R. Superfine, E. Freysz, and Y. R. Shen, "Vibrational Spectroscopy of Water at the Vapor/Water Interface," Phys. Rev. Lett. **70**, 2313–2316 (1993).

[35] V. Ostroverkhov, G. A. Waychunas, and Y. R. Shen, "New information on water interfacial structure revealed by phase-sensitive surface spectroscopy," Phys. Rev. Lett. **94**, 046102 (2005).

[36] H. Groenzin, I. Li, V. Buch, and M. J. Shultz, "The single-crystal, basal face of ice Ih investigated with sum frequency generation," J. Chem. Phys. **127**, 214502 (2007).

[37] Y. R. Shen, "Basic theory of surface sum-frequency generation," J. Phys. Chem. **116**, 15505–15509 (2012).

[38] T. Ishiyama, H. Takahashi, and A. Morita, "Origin of vibrational spectroscopic response at ice surface," J. Phys. Chem. Lett. **3**, 3001 (2012).

[39] Y. R. Shen, "Phase-sensitive sum-frequency spectroscopy," Annual Review of Physical Chemistry **64**, 129–150 (2013).

[40] T. Ohto, K. Usui, T. Hasegawa, M. Bonn, and Y. Nagata, "Toward ab initio molecular dynamics modeling for sum-frequency generation spectra; an efficient algorithm based on surface-specific velocity-velocity correlation function," J. Chem. Phys. **143**, 124702 (2015).

[41] F. Tang, T. Ohto, S. Sun, J. R. Rouxel, S. Imoto, E. H. G. Backus, S. Mukamel, M. Bonn, and Y. Nagata, "Molecular structure and modeling of water-air and ice-air interfaces monitored by sum-frequency generation," Chem. Rev. **120**, 3633–3667 (2020).

[42] I.-F. W. Kuo, C. J. Mundy, B. L. Eggimann, M. J. McGrath, J. I. Siepmann, B. Chen, J. Vieceli, and D. J. Tobias, "Structure and dynamics of the aqueous liquid-vapor interface: A comprehensive particle-based simulation study," J. Phys. Chem. B **110**, 3738–3746 (2006).

[43] C. D. Wick, I.-F. W. Kuo, C. J. Mundy, and L. X. Dang, "The effect of polarizability for understanding the molecular structure of aqueous interfaces," J. Chem. Theory Comput. **3**, 2002–2010 (2007).

[44] A. Morita and B. C. Garrett, "Molecular theory of mass transfer kinetics

and dynamics at gas-water interface," Fluid Dynamics Research **40**, 459 (2008).
[45]F. Sedlmeier, D. Horinek, and R. R. Netz, "Nanoroughness, intrinsic density profile, and rigidity of the air-water interface," Phys. Rev. Lett. **103**, 136102 (2009).
[46]Y. Fan, X. Chen, L. Yang, P. S. Cremer, and Y. Q. Gao, "On the structure of water at the aqueous/air interface," J. Phys. Chem. B **113**, 11672–11679 (2009).
[47]T. Ishiyama and A. Morita, "Analysis of anisotropic local field in sum frequency generation spectroscopy with the charge response kernel water model," J. Chem. Phys. **131**, 244714 (2009).
[48]A. P. Willard and D. Chandler, "Instantaneous Liquid Interfaces," J. Phys. Chem. B **114**, 1954 (2010).
[49]A. Vila Verde, P. G. Bolhuis, and R. K. Campen, "Statics and dynamics of free and hydrogen-bonded oh groups at the air/water interface," J. Phys. Chem. B **16**, 9467–9481 (2012).
[50]T. Ishiyama, A. Morita, and T. Tahara, "Molecular dynamics study of two-dimensional sum frequency generation spectra at vapor/water interface," J. Chem. Phys. **142**, 212407 (2015).
[51]Y. Nagata, T. Hasegawa, E. H. G. Backus, K. Usui, S. Yoshimune, T. Ohto, and M. Bonn, "The surface roughness, but not the water molecular orientation varies with temperature at the water-air interface," Phys.Chem.Chem.Phys. **17**, 23559 (2015).
[52]T. D. Kühne, T. A. Pascal, E. Kaxiras, and Y. Jung, "New Insights into the Structure of the Vapor/Water Interface from Large-Scale First-Principles Simulations," J. Phys. Chem. Lett. **2**, 105–113 (2011).
[53]Y. Nagata, R. E. Pool, E. H. G. Backus, and M. Bonn, "Nuclear quantum effects affect bond orientation of water at the water-vapor interface," Phys. Rev. Lett. **109**, 226101 (2012).
[54]J. Kessler, H. Elgabarty, T. Spura, K. Karhan, P. Partovi-Azar, A. A. Hassanali, and T. D. Kühne, "Structure and Dynamics of the Instantaneous Water/Vapor Interface Revisited by Path-Integral and Ab Initio Molecular Dynamics Simulations," J. Phys. Chem. B **199**, 10079–10086 (2015).
[55]T. Ohto, M. Dodia, J. Xu, S. Imoto, F. Tang, F. Zysk, T. D. Kühne, Y. Shigeta, M. Bonn, and Y. Nagata, "Accessing the accuracy of density functional theory through structure and dynamics of the water-air interface," J. Phys. Chem. Lett. **10**, 4914–4919 (2019).
[56]P. Jungwirth and D. J. Tobias, "Specific Ion Effects at the Air/Water Interface," Chem. Rev. **106**, 1259–1281 (2006).
[57]M. D. Baer, I.-F. W. Kuo, D. J. Tobias, and C. J. Mundy, "Toward a unified picture of the water self-ions at the air-water interface: A density functional theory perspective," J. Phys. Chem. B **118**, 8364–8372 (2014).
[58]C. V. Nguyen, H. Nakahara, and C. M. Phan, "Surface potential of the air/water interface," J. Oleo Science **69**, 519–528 (2020).
[59]Y. Peng, Z. Tong, Y. Yang, and C. Q. Sun, "The Common and Intrinsic Skin Electric-Double-Layer (EDL) and Its Bonding Characteristics of Nanostructures," Applied Surface Science **539**, 148208 (2021).
[60]R. M. Townsend, J. Gryko, and S. A. Rice, "Structure of the liquid-vapor interface of water," J. Chem. Phys. **82**, 4391–4392 (1985).
[61]M. A. Wilson, A. Pohorille, and L. R. Pratt, "Molecular dynamics of the water liquid-vapor interface," J. Phys. Chem. **91**, 4873–4878 (1987).
[62]M. Matsumoto and Y. Kataoka, "Study on liquid-vapor interface of water. i. simulational results of thermodynamic properties and orientational structure," J. Chem. Phys. **88**, 3233–3245 (1988).
[63]R. M. Townsend and S. A. Rice, "Molecular dynamics studies of the liquid-vapor interface of water," J. Chem. Phys. **94**, 2207–2218 (1991).
[64]G. C. Lie, S. Grigoras, L. X. Dang, D. Yang, and A. D. McLean, "Monte carlo simulation of the liquid-vapor interface of water using an ab initio potential," J. Chem. Phys. **99**, 3933–3937 (1993).
[65]J. Alejandre, D. J. Tildesley, and G. A. Chapela, "Molecular dynamics simulation of the orthobaric densities and surface tension of water," J. Chem. Phys. **102**, 4574–4583 (1995).
[66]R. S. Taylor, L. X. Dang, and B. C. Garrett, "Molecular Dynamics Simulations of the Liquid/Vapor Interface of SPC/E Water," J. Phys. Chem. **100**, 11720–11725 (1996).
[67]L. X. Dang and T.-M. Chang, "Molecular dynamics study of water clusters, liquid, and liquid-vapor interface of water with many-body potentials," J. Chem. Phys. **106**, 8149–8159 (1997).
[68]R. Car and M. Parrinello, "Unified Approach for Molecular Dynamics and Density Functional Theory," Phys. Rev. Lett. **55**, 2471–2474 (1985).
[69]D. Marx and J. Hutter, "Ab Initio Molecular Dynamics: Theory and Implemention," Modern Methods and Algorithms of Quantum Chemistry, J.Grotendorst (Ed.) John von Neumann Institute for Computing, Jülich, NIC Series **1**, 301–499 (2000).
[70]R. Car, "Introduction to Density-Functional Theory and Ab-Initio Molecular Dynamics," Quant. Struct. Act. Rel. **21**, 97–104 (2002).
[71]I.-F. W. Kuo and C. J. Mundy, "An Ab Initio Molecular Dynamics Study of the Aqueous Liquid-Vapor Interface," Science **303**, 658 (2004).
[72]T. D. Kühne, M. Krack, F. R. Mohamed, and M. Parrinello, "Efficient and accurate car-parrinello-like approach to born-oppenheimer molecular dynamics," Phys. Rev. Lett. **98**, 066401 (2007).
[73]R. Z. Khaliullin and T. D. Kühne, "Microscopic properties of liquid water from combined ab initio molecular dynamics and energy decomposition studies," Phys. Chem. Chem. Phys. **15**, 15746–15766 (2013).
[74]F. J. Blas, E. M. D. Río, E. D. Miguel, and G. Jackson, "An examination of the vapour-liquid interface of associating fluids using a saft-dft approach," Molecular Physics **99**, 1851–1865 (2001).
[75]S. Pezzotti, D. R. Galimberti, and M.-P. Gaigeot, "2D H-Bond Network as the Topmost Skin to the Air-Water Interface," J. Phys. Chem. Lett. **8**, 3133–3141 (2017).
[76]A. Luzar and D. Chandler, "Hydrogen-Bond Kinetics in Liquid Water," Nature **379**, 55–57 (1996).
[77]F. Giberti and A. A. Hassanali, "The excess proton at the air-water interface: The role of instantaneous liquid interfaces," J. Chem. Phys. **146**, 244703 (2017).
[78]D. Beaglehole and P. Wilson, "Thickness and Anisotropy of the Ice-Water Interface," J. Phys. Chem. **97**, 11053–11055 (1993).
[79]V. P. Sokhan and D. J. Tildesley, "The free surface of water: molecular orientation, surface potential and nonlinear susceptibility," Molecular Physics **92**, 625–640 (1997).
[80]S. Paul and A. Chandra, "Hydrogen bond dynamics at vapour-water and metal-water interfaces," Chem. Phys. Lett. **386**, 218–224 (2004).
[81]A. Morita, "Improved computation of sum frequency generation spectrum of the surface of water," J. Phys. Chem. B **110**, 3158–3163 (2006).
[82]J. Zhao, G. Yao, S. B. Ramisetti, R. B. Hammond, and D. Wen, "Molecular dynamics simulation of the salinity effect on the n-decane/water/vapor interfacial equilibrium," Energy Fuels **32**, 11080–11092 (2018).
[83]A. Serva, S. Pezzotti, S. Bougueroua, D. R. Galimberti, and M.-P. Gaigeot, "Combining ab-initio and classical molecular dynamics simulations to unravel the structure of the 2d-hb-network at the air-water interface," J. Molecular Structure **1165**, 71–78 (2018).
[84]A. Madarasz, P. J. Rossky, and L. Turi, "Excess electron relaxation dynamics at water/air interfaces," J. Chem. Phys. **126**, 234707 (2007).
[85]A. Luzar and D. Chandler, "Structure and hydrogen bond dynamics of water–dimethyl sulfoxide mixtures by computer simulations," J. Chem. Phys. **98**, 8160–8173 (1993).
[86]A. Luzar, "Resolving the Hydrogen Bond Dynamics Conundrum," J. Chem. Phys. **113**, 10663 (2000).
[87]K. ichi Inoue, M. Ahmed, S. Nihonyanagi, and T. Tahara, "Reorientation-induced relaxation of free OH at the air/water interface revealed by ultrafast heterodyne-detected nonlinear spectroscopy," Nature Communications **11**, 5344 (2020).
[88]Y. Rao, Y.-s. Tao, and H.-f. Wang, "Quantitative analysis of orientational order in the molecular monolayer by surface second harmonic generation," J. Chem. Phys. **119**, 5226–5236 (2003).
[89]W. Gan, D. Wu, Z. Zhang, R.-r. Feng, and H.-f. Wang, "Polarization and experimental configuration analyses of sum frequency generation vibrational spectra, structure, and orientational motion of the air/water interface," J. Chem. Phys. **124**, 114705 (2006).
[90]A. Luzar and D. Chandler, "Effect of environment on hydrogen bond dynamics in liquid water," Phys. Rev. Lett. **76**, 928–931 (1996).
[91]A. Chandra, "Effects of Ion Atmosphere on Hydrogen-Bond Dynamics in Aqueous Electrolyte Solutions," Phys. Rev. Lett. **85**, 768–771 (2000).
[92]M. Tarek and D. J. Tobias, "Role of Protein-Water Hydrogen Bond Dynamics in the Protein Dynamical Transition," Phys. Rev. Lett. **88**, 138101 (2002).
[93]S. Pal, B. Bagchi, and S. Balasubramanian, "Hydration Layer of a Cationic Micelle, C10TAB: Structure, Rigidity, Slow Reorientation, Hydrogen Bond Lifetime, and Solvation Dynamics," J. Phys. Chem. B **109**, 12879–12890 (2005).

[94]F. Sciortino and S. L. Fornili, "Hydrogen Bond Cooperativity in Simulated Water: Time Dependence Analysis of Pair Interactions," J. Chem. Phys. **90**, 2786–2792 (1989).
[95]A. K. Soper and M. G. Phillips, "A New Determination of the Structure of Water at 25 °C," Chem. Phys **107**, 47–60 (1986).
[96]J. Teixeira, M. C. Bellisent-Funel, and S. H. Chen, "Dynamics of Water Studied by Neutron Scattering," J. Phys. Condens. Matter **2**, SA105 (1990).
[97]A. Luzar and D. Chandler, "Structure and hydrogen bond dynamics of water-dimethyl sulfoxide mixtures by computer simulations," J. Chem. Phys. **98**, 8160–8173 (1993).
[98]S. Balasubramanian, S. Pal, and B. Bagchi, "Hydrogen-Bond Dynamics Near a Micellar Surface: Origin of the Universal Slow Relaxation at Complex Aqueous Interfaces," Phys. Rev. Lett. **89**, 115505 (2002).
[99]D. Chandler, *Introduction to Morden Statistical Mechanics* (Oxford University press, Oxford, 1987).
[100]The average number of H-bonds in an equilibrium of N water molecules is: $\frac{1}{2}N(N-1)\langle h\rangle$, i.e., $\frac{1}{2}N(N-1)\langle h\rangle \sim N$. It implies that $\frac{1}{2}N\langle h\rangle \sim 1$, or $\langle h\rangle \sim \frac{2}{N}$. Therefore, for a large system, $\langle h\rangle$ is extremely small.
[101]I. Benjamin, "Hydrogen Bond Dynamics at Water/Organic Liquid Interfaces," J. Phys. Chem. B **109**, 13711–13715 (2005).
[102]D. C. Rapaport, "Hydrogen Bonds in Water: Network Organization and Lifetimes," Mol. Phys. **50**, 1151–1162 (1983).
[103]F. W. Starr, J. K. Nielsen, and H. E. Sta, "Hydrogen-Bond Dynamics for the Extended Simple Point-Charge Model of Water," Phys. Rev. E **62**, 579–587 (2000).
[104]D. Chandler, "Roles of Classical Dynamics and Quantum Dynamics on Activated Processes Occurring in Liquids," J. Stat. Phys. **42**, 49–67 (1986).
[105]D. Chandler, "Statistical Mechanics of Isomerization Dynamics in Liquids and the Transition State Approximation," J. Chem. Phys. **68**, 2959–2970 (1978).
[106]F. W. Starr, J. K. Nielsen, and H. E. Stanley, "Hydrogen-bond dynamics for the extended simple point-charge model of water," Phys. Rev. E **62**, 579–587 (2000).
[107]S. Woutersen and H. J. Bakker, "Resonant intermolecular transfer of vibrational energy in liquid water," Nature **402**, 1 (1999).
[108]M. L. Cowan, B. D. Bruner, N. Huse, J. R. Dwyer, B. Chugh, E. T. J. Nibbering, T. Elsaesser, and R. J. D. Miller, "Ultrafast memory loss and energy redistribution in the hydrogen bond network of liquid h_2o," Nature **434**, 199 (2005).
[109]D. Kraemer, M. L. Cowan, A. Paarmann, N. Huse, E. T. J. Nibbering, T. Elsaesser, and R. J. D. Miller, "Temperature dependence of the two-dimensional infrared spectrum of liquid h_2o," PNAS **105**, 437–442 (2008).
[110]T. Yagasaki, J. Ono, and S. Saito, "Ultrafast energy relaxation and anisotropy decay of the librational motion in liquid water: A molecular dynamics study," J. Chem. Phys. **131**, 164511 (2009).
[111]J. R. Schmidt, S. A. Corcelli, and J. L. Skinner, "Pronounced Non-Condon Effects in the Ultrafast Infrared Spectroscopy of Water," J. Chem. Phys. **123**, 044513 (2005).
[112]A. Tokmakoff, "Orientational correlation functions and polarization selectivity for nonlinear spectroscopy of isotropic media. i. third order," J. Chem. Phys. **105**, 1–12 (1996).
[113]Y. L. A. Rezus and H. J. Bakker, "Orientational dynamics of isotopically diluted h2o and d2o," J. Chem. Phys. **125**, 144512 (2006).
[114]H. Bakker and J. L. Skinner, "Vibrational Spectroscopy as a Probe of Structure and Dynamics in Liquid Water," Chem. Rev. **110**, 1498 (2010).
[115]A. Geiger, P. Mausbach, J. Schnitker, R. L. Blumberg, and H. E. Stanley, "Structure and Dynamics of the Hydrogen Bond Network in Water by Computer Simulations," J. Phys. (Paris) **45**, C7–13–C7–30 (1984).
[116]Y. S. Lin, P. A. Pieniazek, M. Yang, and J. L. Skinner, "On the Calculation of Rotational Anisotropy Decay, as Measured by Ultrafast Polarization-Resolved Vibrational Pump-Probe Experiments," J. Chem. Phys. **132**, 174505 (2010).
[117]K. Laasonen, M. Sprik, M. Parrinello, and R. Car, ""ab initio" liquid water," J. Chem. Phys. **99**, 9080–9089 (1993).
[118]R. Khatib, E. H. G. Backus, M. Bonn, M. Perez-Haro, M.-P. Gaigeot, and M. Sulpizi, "Water Orientation and Hydrogen-Bond Structure at the Fluorite/Water Interface," Scientific Reports **6**, 24287 (2016).
[119]R. Khatib, T. Hasegawa, M. Sulpizi, E. H. G. Backus, M. Bonn, and Y. Nagata, "Molecular Dynamics Simulations of SFG Librational Modes Spectra of Water at the Water-Air Interface," J. Phys. Chem. C **120**, 18665–18673 (2016).
[120]R. Khatib and M. Sulpizi, "Sum Frequency Generation Spectra from Velocity-Velocity Correlation Functions," J. Phys. Chem. Lett. **8**, 1310–1314 (2017).
[121]S. Goedecker, M. Teter, and J. Hutter, "Separable dual-space gaussian pseudopotentials," Phys. Rev. B **54**, 1703–1710 (1996).
[122]C. Hartwigsen, S. Goedecker, and J. Hutter, "Relativistic separable dual-space gaussian pseudopotentials from H to Rn," Phys. Rev. B **58**, 3641–3662 (1998).
[123]M. Krack, "Pseudopotentials for H to Kr optimized for gradient-corrected exchange-correlation functionals," Theor. Chem. Acc. **114**, 145–152 (2005).
[124]A. D. Becke, "Density-functional exchange-energy approximation with correct asymptotic behavior," Phys. Rev. A **38**, 3098 (1988).
[125]C. Lee, W. Yang, and R. G. Parr, "Development of the colic-salvetti correlation-energy formula into a functional of the electron density," Phys. Rev. B **37**, 785 (1988).
[126]S. Grimme, J. Antony, S. Ehrlich, and H. Krieg, "A Consistent and Accurate Ab Initio Parametrization of Density Functional Dispersion Correction (DFT-D) for the 94 Elements H-Pu," J. Chem. Phys. **132**, 154104 (2010).
[127]J. Klimeš and A. Michaelides, "Perspective: Advances and Challenges in Treating van der Waals Dispersion Forces in Density Functional Theory," J. Chem. Phys. **137**, 120901–120912 (2012).
[128]J.-B. Lu, D. C. Cantu, M.-T. Nguyen, J. Li, V.-A. Glezakou, and R. Rousseau, "Norm-Conserving Pseudopotentials and Basis Sets To Explore Lanthanide Chemistry in Complex Environments," J. Chem. Theory Comput. **15**, 5987–5997 (2019).
[129]J. VandeVondele, M. Krack, F. Mohamed, M. Parrinello, T. Chassaing, and J. Hutter, "Quickstep: Fast and accurate density functional calculations using a mixed gaussian and plane waves approach," Comput. Phys. Commun. **167**, 103–128 (2005).
[130]T. D. Kühne, M. Iannuzzi, M. Del Ben, V. V. Rybkin, P. Seewald, F. Stein, T. Laino, R. Z. Khaliullin, O. Schütt, F. Schiffmann, D. Golze, J. Wilhelm, S. Chulkov, M. H. Bani-Hashemian, V. Weber, U. Borštnik, M. Taillefumier, A. S. Jakobovits, A. Lazzaro, H. Pabst, T. Müller, R. Schade, M. Guidon, S. Andermatt, N. Holmberg, G. K. Schenter, A. Hehn, A. Bussy, F. Belleflamme, G. Tabacchi, A. Glöß, M. Lass, I. Bethune, C. J. Mundy, C. Plessl, M. Watkins, J. VandeVondele, M. Krack, and J. Hutter, "Cp2k: An electronic structure and molecular dynamics software package - quickstep: Efficient and accurate electronic structure calculations," J. Chem. Phys. **152**, 194103 (2020), https://doi.org/10.1063/5.0007045.
[131]G. Lippert, J. Hutter, and M. Parrinello, "The gaussian and augmented-plane-wave density functional method for ab initio molecular dynamics simulations," Theor. Chem. Acc. **103**, 124 (1999).
[132]G. J. Martyna, M. L. Klein, and M. Tuckerman, "Nosé-hoover chains: The canonical ensemble via continuous dynamics," J. Chem. Phys. **97**, 2635 (1992).

Appendix A: Hydrogen bond correlation functions

Using a geometric criterion of HB, Luzar and Chandler[90] have pioneered the analysis of HB dynamics of pure water, and subsequently, such analysis has been extended to more complex systems, e.g., electrolytes[91], protein[92], and micellar surfaces[93]. In the criterion, two water molecules are H-bonded if their inter-oxygen distance $r_{\rm OO}$ is less than the cutoff radius[94] $r_{\rm OO}^{\rm c} = 3.5$ Å and the H-O$\cdots$O angle ϕ is less than cutoff angle $\phi^{\rm c} = \pi/6$[95–98]. We denote it as the acceptor-donor-hydrogen (ADH) criterion. For comparison, we also use another HB criterion: $r_{\rm OO}$ is less than $r_{\rm OO}^{\rm c}$, and the O-H$\cdots$O included angle θ is greater than cutoff angle $\theta^{\rm c} = 2\pi/3$[25]. We denote this HB criterion as the acceptor-hydrogen-donor (AHD) criterion.

We use a configuration $r(t)$ to denote the positions of all the atoms in the system at time t. Either of the criteria above allows one to define an HB population $h[r(t)] = h(t)$, which equals 1 when a tagged pair of molecules are H-bonded, and 0 otherwise. The fluctuation in $h(t)$ from its time-independent equilibrium average is defined by[99] $\delta h = h(t) - \langle h\rangle$. The probability that a *specific* tagged pair of molecules is H-bonded in a large system is extremely small[100], then $\delta h(t) = h(t)$. Therefore, the correlation of $\delta h(t)$ can be written as

$$\langle \delta h(0)\delta h(t)\rangle = \langle h(0)h(t)\rangle,$$

where the averaging $\langle\cdots\rangle$ is to be performed over the ensemble of initial conditions.

The correlation function $c(t) = \langle h(0)h(t)\rangle/\langle h\rangle$ describes the structural relaxation of H-bonds[91,101]. Here the average $\langle h\rangle$ of the HB population is the probability that a pair of randomly chosen water molecules in the system is H-bonded at any time t. The function $c(t)$ measures correlation in $h(t)$ independent of any possible bond-breaking events, and it relaxes to zero when t is large[102].

Because the thermal motion can cause distortions of H-bonds from the perfectly tetrahedral configuration, water molecules show a librational motion on a time scale of ~ 0.1 ps superimposed to rotational and diffusional motions (> 1 ps), which causes a time variation in interaction parameters. A new HB population $h^{(\rm d)}(t)$ was also defined to obviate the distortion of real HB dynamics due to the above geometric definition[91,94]. It is 1 when the inter-oxygen distance of a particular tagged pair of water molecules is less than $r_{\rm OO}^{\rm c}$ at time t, and 0 otherwise. The H-bonds between a tagged molecular pair that satisfy the condition $h^{(\rm d)}(t) = 1$ may have been broken, but they may more easily form H-bonds again. The correlation function

$$n(t) = \langle h(0)[1-h(t)]h^{(\rm d)}(t)\rangle/\langle h\rangle \tag{A1}$$

represents the probability at time t that a tagged pair of initially H-bonded water molecules are unbonded but remain separated by less than $r_{\rm OO}^{\rm c}$[91].

The rate of HB relaxation to equilibrium is characterized by the reactive flux[86]

$$k(t) = -\frac{{\rm d}c(t)}{{\rm d}t}, \tag{A2}$$

which quantifies the rate that an initially present HB breaks at time t, independent of possible breaking and reforming events in the interval from 0 to t. Therefore, $k(t)$ measures the effective decay rate of an the initial set of H-bonds[99]. For bulk water, a ~ 0.2-ps transient period exists, during which $k(t)$ changes quickly from its initial value[103]. However, at longer times, $k(t)$ is independent of the HB definitions.

The dynamic evolution of HB population correlation functions, $c(t)$ and $c^{(\rm s)}(t)$, in the two scenarios, is shown in Fig. A6a and b, respectively. This figure applies the AHD criteria to H-bonds. A critical thickness d_f (equal to or greater than 4.0 (Å)) exists. Beyond this thickness, the time evolution curves of the correlation function $c(t)$ and $c^{(\rm s)}(t)$ do not significantly change with further increases in d.

A comparison between the two scenarios shows that in scenario 2, the correlation function $c^{(\rm s)}(t)$ decays faster than in scenario 1. This is visually indicated by a black directed line segment in the figure. This observation is consistent with conclusions drawn from another criterion, the ADH criterion, as we have shown in the main text.

The result, where $c^{(\rm s)}(t)$ decays faster in scenario 2 compared to $c(t)$ in scenario 1, aligns with findings from the ADH standard. This suggests a level of agreement between the different criteria applied to analyze the air-water interface.

Appendix B: Hydrogen bond breaking and reforming rate constants

Assume that each HB acts independently of other H-bonds[86,90], and due to the detailed balance condition, one obtains $\tau_{\rm HB} = (1-\langle h\rangle)/k$, where k is the rate constant of breaking an HB, i.e., the forward rate constant[104,105]. Correspondingly, the backward rate constant k' is represented by the rate constant from the HB-*on* state to the HB-*off* state for a tagged pair of molecules. Based on the functions (see Appendix A) $n(t)$, $h(t)$, $h^{(\rm d)}(t)$, and $k(t)$, Khaliullin and Kühne [73] have obtained the ratio k/k' of HB breaking and reforming rate constants in bulk water, and then the lifetime and relaxation time of H-bonds from simulations. Here, for the air-water interface, we obtain the optimal solution range of k and k' from the relationship between the reactive flux $k(t)$ and the correlation functions $c(t)$ and $n(t)$:

$$k(t) = kc(t) - k'n(t). \tag{B1}$$

We obtain the optimal value of the rate constants, k and k', by the least squares fit of $k(t)$, $c(t)$, and $n(t)$ beyond the transition phase. The function $c(t)$ is regarded as a column vector composed of $(c_1,\cdots,c_P)^{\rm T}$, and is denoted as $\mathbf{c}$, with c_i representing the value of correlation $c(t)$ at $t = i$. Similarly, $n(t)$ and $k(t)$ can also be denoted as $\mathbf{n}$ and $\mathbf{k}$, respectively. Then, the rate constants k and k' are determined from the matrix $\mathbf{A} = \begin{bmatrix}\mathbf{c} & \mathbf{n}\end{bmatrix}$:

$$\begin{bmatrix} k \\ -k' \end{bmatrix} = (\mathbf{A}^{\rm T}\mathbf{A})^{-1}\mathbf{A}^{\rm T}\mathbf{k}. \tag{B2}$$

For bulk water and the air-water interface, the optimal k and k' are reported in Table B2 and B3. To obtain k and k',

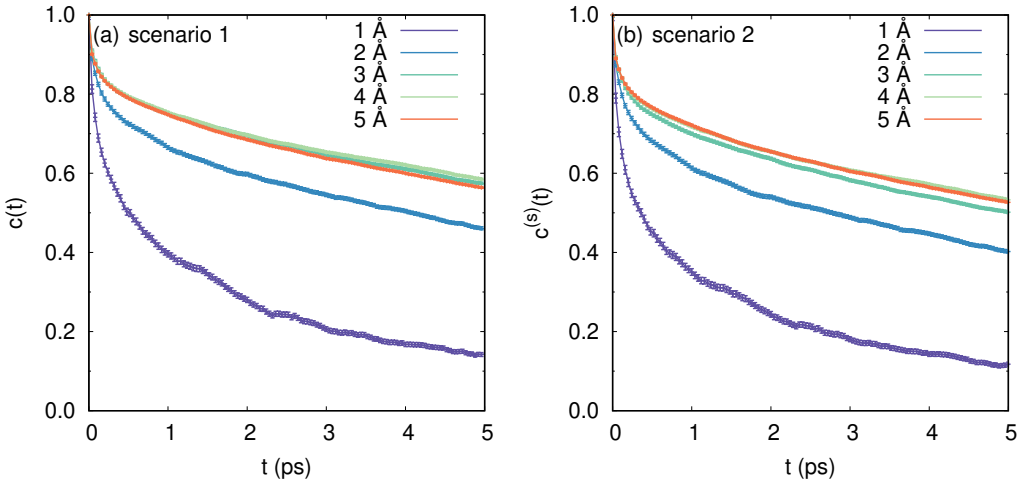

FIG. A6. The $c(t)$ and $c^{(s)}(t)$ for interface H-bonds with different thickness d obtained from the AHD criteria: (a) LC; (b) IHB. In scenario 1, the sampling is performed every 4 ps.

TABLE B2. The rate constants k and k' for the bulk water and the air-water interface (the time region $0.2 < t < 2$ (ps)).

Criterion	k (b)[a]	k' (b)	τ_{HB} (b)[b]	k (i)	k' (i)	τ_{HB} (i)
ADH	0.296	0.988	3.380	0.323	0.765	3.101
AHD	0.288	1.149	3.470	0.314	0.887	3.184

[a] The unit for k (k') is ps^{-1}. b: bulk; i: interface.
[b] The unit for $\tau_{HB} = 1/k$) is ps.

TABLE B3. The k and k' for the bulk water and the air-water interface (the time region $2 < t < 12$ (ps)).

Criterion	k (b)	k' (b)	τ_{HB} (b)	k (i)	k' (i)	τ_{HB} (i)
ADH	0.115	0.039	8.718	0.157	0.068	6.372
AHD	0.105	0.047	9.496	0.155	0.088	6.472

we perform the fitting in short and long-time regions, respectively. Since HB dynamics show different relaxation behaviors in the time of ~ 1 ps and in that greater than ~ 1 ps[106], we will fit the short and long time intervals respectively. We note that in the long time region ($2 < t < 12$ (ps)), the value of HB lifetime τ_{HB} is larger than that in short one ($0.2 < t < 2$ (ps)), no matter for the bulk water or the air-water interface. A larger τ_{HB} value means that the distance between a pair of water molecules stays within r^c_{OO} for a longer time.

Appendix C: Details of Scenario 1: the LC method

In the LC scenario, to obtain interface HB dynamics, we use molecule sampling at the instantaneous interface. Let T_e be the time it takes for all water molecules in the simulation box to traverse the interface and bulk phase. If the trajectory length t_{traj} satisfies the condition $\tau_{HB} \ll t_{traj} \ll T_e$, we sample time points t_i ($i = 1, \cdots, M$) that are evenly spaced on the trajectory, then obtain interface HB dynamics using the following procedure:

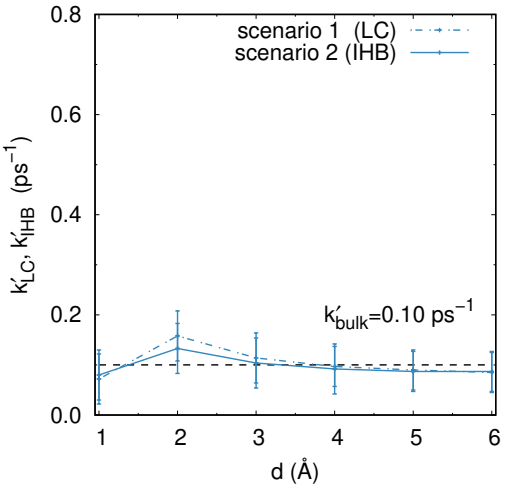

FIG. B7. The d-dependence of the rate constant k'_{IHB} and k'_{LC}, obtained by the IHB (solid lines) and the Luzar-Chandler (dot-dashed lines) methods, respectively. The corresponding reaction rate k'_{bulk} for bulk water is also represented as dashed lines. The ADH criterion of H-bonds is used and the fits are carried on the time region $0.2 < t < 12$ (ps).

1. For each sampling time t_i, define an interface with a thickness d (see Fig. 1). Then, select a set S_i of water molecules in the interfacial layer $\mathscr{I}(d;t)$, i.e., $\mathbf{r}(t_i) \in \mathscr{I}(d;t)$, and calculate the correlation functions $c(t)$, $n(t)$ and $k(t)$ through t_{traj} for these water molecules.

2. Calculate average functions of the correlation functions $c(t)$, $n(t)$, and $k(t)$ respectively over all sampling time points and all trajectories.

3. Calculate reaction rate constants of breaking and reforming in the interfacial layer $\mathscr{I}(d;t)$ by Eq. B1.

In scenario 1, the sampling is performed every 4 ps.

Appendix D: Rotational anisotropy decay of OH stretch at the water/vapor interface

We examine the results for the water interface thickness from the interfacial HB dynamics by polarization anisotropy decay of OH stretch. The polarization anisotropy decay of the OH stretch can also provide information on the dynamics of water [107–110]. We assume that the anisotropy decay $R(t)$ is only due to the orientational relaxation of water molecules. Within the Condon approximation [111], it is directly related to the orientational correlation function $C_2(t)$[110,112–114] through $R(t) = \frac{2}{5}C_2(t)$. The $C_2(t)$ is given by the rotational time-correlation function

$$C_2(t) = \langle P_2(\hat{u}(0)\cdot\hat{u}(t))\rangle, \tag{D1}$$

where $P_2(x)$ is the second-order Legendre polynomial [115], i.e., $P_2(x) = \frac{1}{2}(3x^2-1)$, $\hat{u}(t)$ is the time-dependent unit vector of the transition dipole, and $\langle\rangle$ indicate equilibrium ensemble average [116]. In our simulations, we concentrate on water molecules and consider a unit vector that is directed along the OH bond.

For the air-water interface, using the method in section II, we first obtain the instantaneous interface with thickness $d = 1,\cdots,6$ (Å). Then, for each value of d, the LC method is used to obtain $C_2(t)$ for water molecules at the air-water interface.

Here we introduce a fitting with an exponential and provide a decay time τ_2, i.e., $C_2(t) = Ae^{-t/\tau_2}$, with $A = 1.0$ for different thickness values, and the d-dependence of $C_2(t^*)$ and $\tau_2(t^*)$ is shown in Fig. 5. When the interface thickness d is smaller than 4.0 (Å), the decay time τ_2 increases linearly with d. The OH orientational relaxation time τ_2 for the neat water surface is from 1.4 to 2.0 (ps), with std. error $\delta d = 0.1$ (ps), which is consistent with the vibrational relaxation time of the free OH for the neat water[87].

Similar to the correlation functions, $c(t)$ and $k(t)$, for interfacial water molecules, as d increases, τ_2 converges to a fixed value, which characterizes the decay time of the orientation relaxation process of OH bonds in bulk water. From the convergence trend of τ_2 in Fig. 5(b), we find that at the interface with a thickness greater than 4.0 Å, the OH orientation relaxation of the air-water interface is no longer different from bulk water.

Appendix E: Computational Methods

To describe the subtleties of H-bonding in water[117], we have performed DFTMD simulations[69] for bulk water and the air-water interface. The simulations make use of technologies that have been successfully tested on water and solutions[118–120], namely the Goedecker-Teter-Hutter (GTH) pseudopotentials[121–123], Generalised Gradient Approximation (GGA) of the exchange-correlation functional[124,125], and dispersion force correction, DFT-D3[126,127]. By eliminating the strongly bound core electrons, the GTH pseudopotentials reduce the number of occupied electronic orbitals that have to be treated in an electronic structure calculation. There are dual-space Gaussian-type pseudopotentials that are separable and satisfy a quadratic scaling to system size[128]. The GGA functionals generally describe the dipole and quadruple moments of the molecules quite well, and the DFT-D3 correction treats the van der Waals dispersion forces and improves the structural properties without more computational cost and thus can be used for the air-water interface.

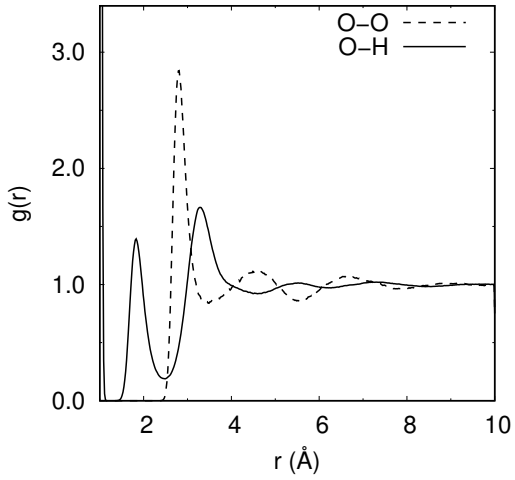

FIG. E1. The partial radial distribution functions (RDFs) for the simulated bulk water system.

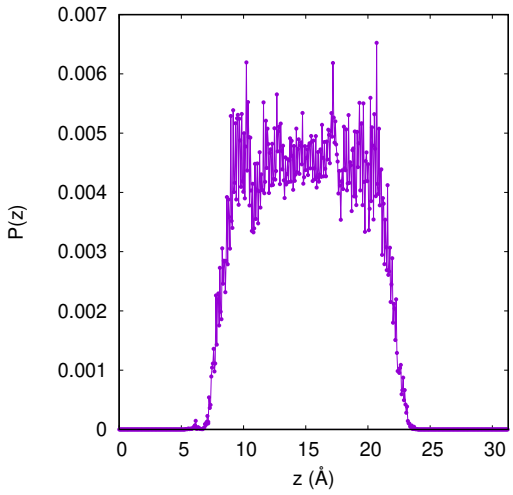

FIG. E2. Probability distribution $P(z)$, along the z-axis, of H_2O in the slab.

The DFTMD calculation is implemented by an NVT code that is implemented in the CP2K/QUICKSTEP package[129,130]. The BLYP XC functional, which consists of Becke non-local exchange[124] and Lee-Yang-Parr correlation[125] has been employed. The electron-ion interactions are described by GTH pseudopotentials[122,131]. A Gaussian basis for the wave functions and an auxiliary plane wave basis set for the density is used in this scheme. The DZVP-GTH basis set is used for all atoms and a cutoff of 280 Ry is chosen for the charge density[129]. The Nosé-Hoover chain thermostat[132] is

used to conserve the temperature at 300 K. The simulation for the air-water interface uses a time step of 0.5 fs.

The bulk water system consisted of 128 water molecules in a periodic box of size $15.64 \times 15.64 \times 15.64$ Å^3, and with a density of 1.00 g cm^{-3}. The slab consisted of 128 water molecules in a periodic box of size $15.64 \times 15.64 \times 31.28$ Å^3. The length of each trajectory is 60 (ps). The RDFs $g_{\mathrm{OO}}(r)$ and $g_{\mathrm{OH}}(r)$ for the bulk water systems are shown in Fig. E1. The probability distribution of O and H atoms in the simulated model of the air-water interface is shown in Fig. E2.